

Critical heat flux in thin, uniform particle coatings

G.-S. Hwang, M. Kaviany *

Department of Mechanical Engineering, University of Michigan Ann Arbor, MI 48109-2125, USA

Received 25 May 2005; received in revised form 16 September 2005

Available online 22 November 2005

Abstract

Pool boiling on thin, uniform porous coatings is examined experimentally using different copper particle diameters (between 40 and 80 μm), fabrications (loosely packed, shaken, or pressed), and particle characteristics (solid or porous particle) with coating thickness varying between 3 and 5 particle diameters. The results show that the critical heat flux (CHF) is about 1.8 times for all the coatings, while the pre-CHF regime shows variations. We suggest that the presence of the thin, uniform porous coating influences the hydrodynamic (macroscale) stabilities such that statistically the critical Rayleigh–Taylor wavelength decreases and/or the vapor area fraction increases in a manner to statistically cause a decrease in the dominant interfacial wavelength. By the CHF experimental results, it is postulated that for a 2-fold increase in CHF, the wavelength in the Zuber CHF model is nearly one-fourth of that for plain surface, or the area of the vapor channels increases by $2^{2/3}$ (compared to plain surface).

© 2005 Elsevier Ltd. All rights reserved.

Keywords: Porous coating; Enhanced pool boiling; Critical heat flux; Particle coating

1. Introduction

Various coatings of boiling surfaces have been studied to increase the critical heat flux (CHF) q_{CHF} , and/or to reduce the surface superheat, $T_s - T_{\text{lg}}$, at a given surface heat flux q , compared to the performance of a plain surface [1–11]. The enhancement is attributed to the combinations of complex flow phenomena and the fluid/solid thermo-physical properties, and the coating geometrical parameters.

Zuber originally developed the CHF model for a uniform temperature plain surface by using the hydrodynamic stability theories [12], which have macroscale point of view compared to the particle coating scale. Using this model, modulated porous-layer coatings were developed to increase CHF on the surface by changing the wavelength (Rayleigh–Taylor, or Zuber) of the onset of hydrodynamic instabilities from the fluid thermophysical properties into

that controlled by the porous, wavy (modulated) coating. The Zuber $q_{\text{CHF,Z}}$ and wavelength are [11]

$$q_{\text{CHF,Z}} = \Delta h_{\text{lg}} \left(\frac{\pi^3 \sigma \rho_{\text{g}}}{288 \lambda_{\text{RT}}} \right)^{1/2}, \quad (1)$$

where

$$\lambda_{\text{RT}} = 9 \left[\frac{\sigma}{g(\rho_{\text{l}} - \rho_{\text{g}})} \right]^{1/2}. \quad (2)$$

By focusing on the particle (micro) scale and transport in the coating, a semi-empirical q_{CHF} model has also been suggested for uniform porous-layer coatings as [14]

$$q_{\text{CHF,u}} = 0.52 \epsilon^{2.28} \Delta h_{\text{lg}} \left[\frac{2\sigma \rho_{\text{l}} \rho_{\text{g}}}{(\rho_{\text{l}} + \rho_{\text{g}}) d_{\text{br}}} \right]^{1/2}, \quad (3)$$

where d_{br} is the diameter of the breakthrough bubble (the onset of bubble penetration through a uniform porous coating; initially the layer is fully saturated with liquid, and then subjected to upwardly forced gas flow), and is determined experimentally. This relation suggests that the

* Corresponding author. Tel.: +1 734 936 0402; fax: +1 734 647 3170.
E-mail address: kaviany@umich.edu (M. Kaviany).

Nomenclature

| | |
|------------------------|---|
| a | area ratio |
| d | particle diameter (m) |
| g | gravitational acceleration (m/s^2) |
| Δh_{lg} | enthalpy of vaporization (J/kg) |
| q | heat flux (W/m^2) |
| R | base radius (m) |
| T | temperature (K) |

Greek symbols

| | |
|------------|-----------------------------|
| δ | coating thickness (m) |
| ϵ | porosity |
| ρ | density (kg/m^3) |
| λ | wavelength |
| σ | surface tension (N/m) |

Subscripts

| | |
|-----|--|
| b | base of characteristic hydrodynamic cell |
| br | breakthrough |
| CHF | critical heat flux |
| g | gas (vapor), gas flow |
| KH | Kelvin–Helmholtz |
| l | liquid |
| lg | liquid–vapor, or saturation |
| p | plain |
| RT | Rayleigh–Taylor |
| s | saturation |
| u | uniform porous-layer coating |
| Z | Zuber |

critical (hydrodynamic) wavelength, which in turn determines the CHF, depends on breakthrough bubble diameter [11].

While (a) the extension of the Zuber theory to the modulated surface coatings does not allow for the prediction of q_{CHF} for uniform coatings, and (b) Eq. (3) requires a measured value of d_{br} , we will examine the newly obtained experimental results under these two models. Here we report on experimental results for uniform particle coatings, and find a trend showing no significant dependence of q_{CHF} on the particle size and other surface characteristics.

2. Experiment

Eight uniform porous-layer coatings were fabricated by Outokumpu, Finland. Their characteristics are listed in Table 1, and are referred to as surfaces # 5, # 43, # 45–47, and # 49–51. The porosity of all the coatings is expected to be around 0.4, due to random arrangements [15]. The average particle diameters range from 40 to 80 μm , and the thicknesses of the coatings range from 3 to 5 particle layers. The particles in surface # 43 are made

by gas atomization, and surfaces # 45 and # 46 have porous particles referred to as HydroCopper (Outokumpu, Finland). The porous particles create a double-porosity coating (one within the particles and the other among the particles). The particles in surface # 49 are shaken before brazing, and in surface # 50 they are pressed before brazing. Surface # 51 includes fine particles within the coating. The other two surfaces, # 5 and # 47, are loosely coated with copper particles. The surface # 10, which consists of particles of 200 μm diameter, and the highly polished plain surface, were tested and reported in [11]. Fig. 1 shows the micrographs of the cross section of several coatings.

The experimental apparatus was reported in [11]. All the coating surfaces are provided on a thin copper disk of 5.08 cm diameter, and are soldered on a cylindrical solid copper base 5.08 cm in diameter and 4.5 cm in length. The coated surface soldered to the copper base is then attached to a large cylindrical, insulated copper thermal mass using a clamp. A high thermal conductivity paste is used to reduce the thermal contact resistance. A glass reservoir and a steel base plate are fabricated to seal around the test surface and to hold the liquid pool. A copper pipe coil condenser is used, and a flexible plastic cap is used to close the system and to maintain an atmospheric pressure.

Two electrical heaters of 1.3 kW and 1.0 kW are used to provide heat to for the lower half of the insulated copper thermal mass. The heat flows through the top half of the thermal mass and then through the test piece. Along the outside of the glass reservoir, a flexible heater is used to maintain the temperature near the fluid (*n*-pentane) saturation temperature. Five E-type thermocouples are aligned axially at measured locations, two in the thermal mass and three in the test piece. The three in the test piece are set apart 1 cm from each other. The closest one to the surface is located at 2 mm below the surface. The heat flux is calculated by applying the Fourier conduction law, where the thermal conductivity of the copper is evaluated at the

Table 1
Uniform porous-layer coating fabricated by Outokumpu, Finland, using brazed copper particles

| Coatings | $\langle d \rangle$ (μm) | δ/d | $\langle \epsilon \rangle$ | Description |
|----------|---------------------------------------|------------|----------------------------|--------------------------------|
| Plain | – | – | 1 | Plain surface |
| # 5 | 80 | 5 | 0.4 | Loose particles |
| # 10 | 200 | 3 | 0.4 | Loose particles |
| # 43 | 50 | 5 | 0.4 | Gas atomized particles |
| # 45 | 60 | 3 | 0.4 | HydroCopper (porous) particles |
| # 46 | 60 | 5 | 0.4 | HydroCopper (porous) particles |
| # 47 | 40 | 4 | 0.4 | Loose particles |
| # 49 | 40 | 3 | 0.4 | Shaken particles |
| # 50 | 40 | 3 | 0.4 | Pressed particles |
| # 51 | 40 | 4 | 0.4 | Includes fine particles |

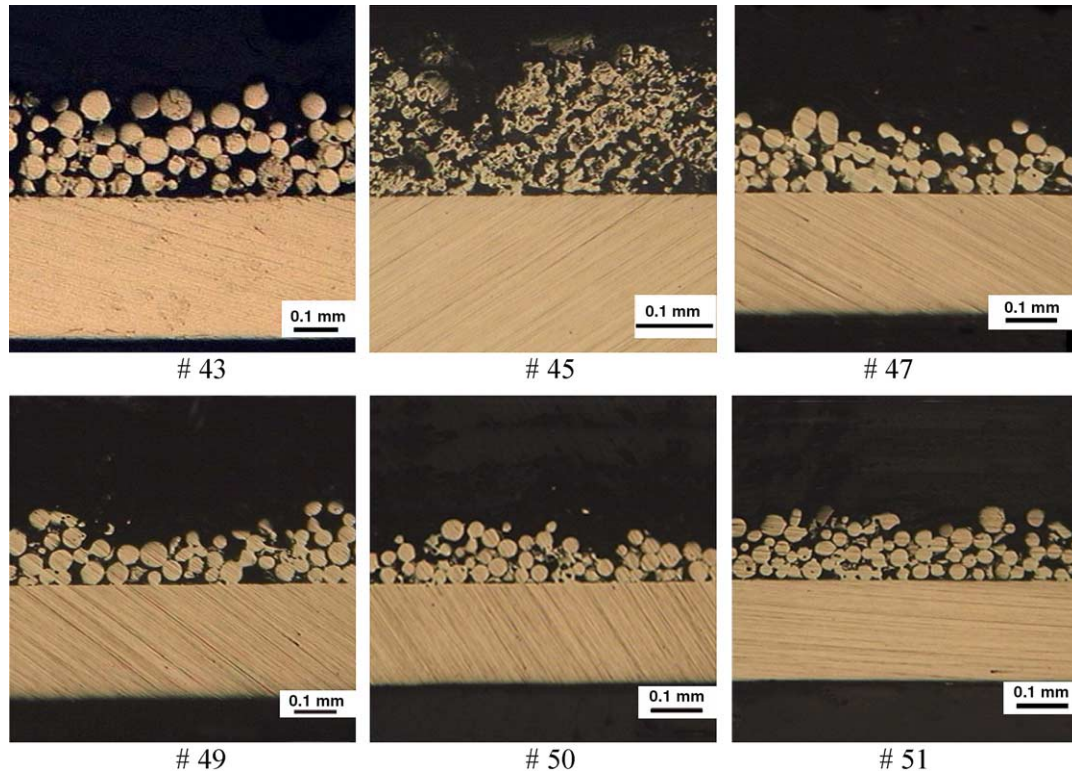


Fig. 1. Micrograph of cross section for various uniform porous-layer coatings used. They show variations in coating thickness, as well as the porous particles (double porosity).

average temperature. The surface temperature underneath the porous coating is determined by extrapolation from the thermocouples in the test piece.

In the pre-CHF regime, the heat flux and the superheat are measured after the system reaches quasi-steady-state condition defined by observing (recording) constant temperature for each thermocouple for at least 2 min. The critical heat flux q_{CHF} is postulated to have occurred at the last observed quasi-steady-state measurement interval (just before the transition to film boiling is observed). This observation is noted as a sudden, runaway temperature jump.

3. Results and discussion

Experimental results for the surfaces with uniform porous-layer coatings have been obtained for the heat flux q versus the surface superheat $T_s - T_{\text{lg}}$, up to the critical heat flux q_{CHF} . About 10 data points are obtained for each coating with a surface superheat of less than 40 K. The measured values of q_{CHF} , and the surface superheat for $q = 245 \text{ kW/m}^2$ (which is critical heat flux $q_{\text{CHF,p}}$ of the plain surface), are summarized in Table 2, where the plain surface and surface # 10 from [11] are also listed.

To investigate the effect of average diameter of particles on the CHF and the surface superheat, the results for surfaces # 5, # 10, and # 47 are compared, along with those for the plain surface in Fig. 2. These three surfaces are loosely coated with almost the same layer thicknesses of

Table 2

| Measured q_{CHF} and $T_s - T_{\text{lg}}$ for $q = 245 \text{ kW/m}^2$ (plain surface $q_{\text{CHF,p}}$) | | | | |
|--|--------|---|---------------------------------------|-----------------------------------|
| Coatings | Symbol | $[T_s - T_{\text{lg}}]_{q_{\text{CHF,p}}}$ (°C) | q_{CHF} (kW/m ²) | $q_{\text{CHF}}/q_{\text{CHF,p}}$ |
| Plain | ▼ | 34 | 245 | 1 |
| # 5 | ▷ | 3.8 | 412 | 1.68 |
| # 10 | ◆ | 9 | 480 | 1.96 |
| # 43 | ▽ | 2.2 | 454 | 1.85 |
| # 45 | ◇ | 5.3 | 441 | 1.8 |
| # 46 | △ | 5.7 | 467 | 1.9 |
| # 47 | ○ | 3.8 | 430 | 1.75 |
| # 49 | ● | 2.5 | 464 | 1.89 |
| # 50 | ▲ | 2.2 | 454 | 1.85 |
| # 51 | □ | 3.3 | 398 | 1.62 |

3–5 particles ($\delta/d = 3\text{--}5$). As expected, the porous-layer coated surfaces offer smaller superheats than the plain surface. The three coated surfaces have nearly the same superheats in the pre-CHF regime of 50–100 kW/m², but in the heat flux of more than 100 kW/m², the surfaces with the relatively larger diameter of particles (i.e., surface # 5 and # 10) show more increased superheat than the smaller one (i.e., surface # 47). This is consistent with the dominance of conduction across the layer, based on an effective conductivity and an average coating thickness. Then, the smaller the particle diameter is, the smaller the average coating thickness becomes (for nearly the same number of particles across the layer). It has been observed previously that q_{CHF} reaches a plateau when the coating thickness is in the range of 3–4 particle diameters, with the

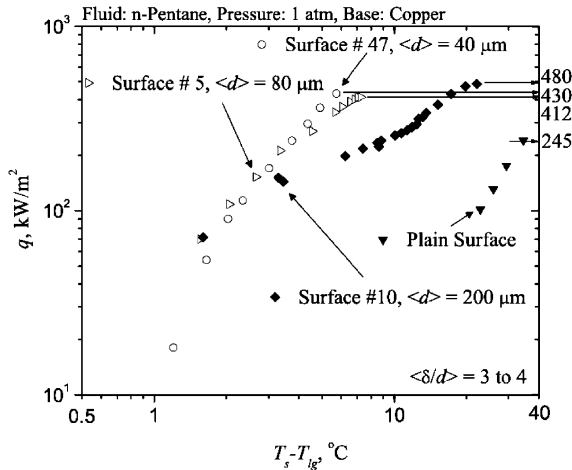


Fig. 2. Effect of particle size on the q versus the superheat curve. The plain surface results are shown.

particle diameter having a small effect on the performance [13]. The results for the CHF are within a narrow range, $q_{CHF} = 412\text{--}480 \text{ kW/m}^2$ (which is about 1.8 times as high as that of the plain surface), and this variation is within the experimental uncertainties. The surface superheat in the pre-CHF regime shows a coating dependency, through coating thickness and the effective thermal conductivity.

For study of the effect of porous particles on the CHF and the surface superheat, the results for the two surfaces coated with porous particles, # 45 and # 46, are compared with the plain surface, and the least superheated surface # 43 in Fig. 3. In the pre-CHF regime, the surfaces with porous particles (surfaces # 45 and # 46) show higher superheat compared to the surface with solid particles (surface # 43). Since these fine pores within the particles do not contribute to decrease the surface superheat, this confirms that an evaporation occurs at the interface of thin liquid films covering the particles, as postulated in [11], and but

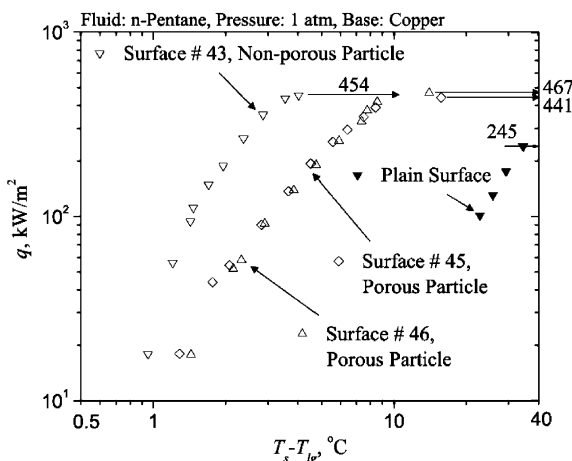


Fig. 3. Effect of porous particles on the q versus the superheat curve. The plain surface and non-porous (solid) particle results are shown.

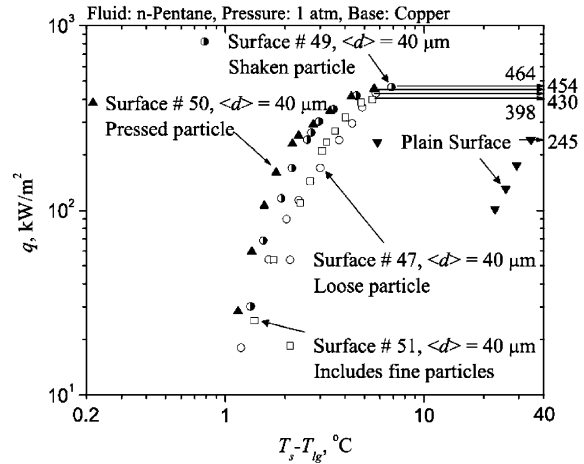


Fig. 4. Effect of various coating on the q versus the superheat curve. The plain surface results are compared.

not by bubble nucleation mechanisms. The increased surface superheat can be due to the extra contact resistance between the porous particles and the heated surface. It may also be caused by the higher porosity which reduces the effective conductivity within the uniform porous layer [15]. The results of the CHF also show that q_{CHF} is nearly independent of the particle characteristics of these thin and uniform porous-layer coatings.

To understand the effect of the various coating characteristics on the CHF and the surface superheat, the experimental results of the surfaces # 47 and # 49–51, including the plain surface are shown in Fig. 4. The results show an enhanced performance compared to the plain surface. For the surface superheat, the difference among the coatings is a maximum of 1 K, at a given heat flux. The enhanced q_{CHF} is within a relatively narrow range of $q_{CHF} = 398\text{--}464 \text{ kW/m}^2$ which is also nearly 1.8 times as high as the plain surface. This suggests that the surfaces with differently fabricated particle coatings show nearly the same CHF and the surface superheat.

As an example, the hysteresis is observed for surface # 50 in the q -increasing and q -decreasing branches as shown in Fig. 5. The higher surface superheat of the q -decreasing branch is due to the trapped vapor, which decreases the effective conductivity [15]. Similar results are expected for other surfaces.

The results for all coatings summarized in Table 2, indicate that q_{CHF} for all the thin, uniform porous-layer coatings range from 398 to 480 kW/m^2 (with n -pentane), which is on average 1.8 times as high as that of the plain surface. With the semi-empirical relation, Eq. (3), the experimental results show that the breakthrough bubbling diameter does not change with the particle size nor with other coating characteristics. In these experiments, the uniform porous-layers result in nearly the same breakthrough bubbling diameter of nearly 200 μm . Note that this is considered as microscale for vapor compared to the critical hydrodynamic wavelength.

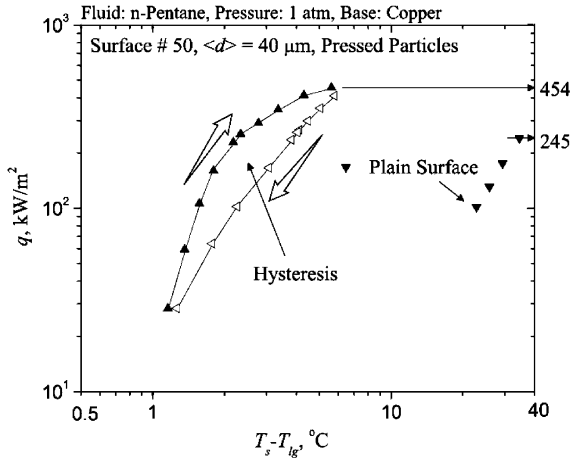


Fig. 5. Observed hysteresis in the q -increasing and q -decreasing branches.

In the Zuber hydrodynamic stability theory for the plain surface, the area portion of an evaporating vapor on the heated surface and the critical Rayleigh–Taylor wavelength are the crucial parts to understand the CHF mechanisms. Fig. 6(a) and (b) show these two key parameters affecting the CHF in the Zuber hydrodynamic stability theory. As shown in Fig. 6(a) and (b), Zuber idealized the gas phase as cylindrical vapor flow channels of area $A_g = \pi R_g^2$, where radius $R_g = a\lambda_b$ and a is to be determined by the ratio of R_g/λ_b , where λ_b is a base length scale of the fluid (for unit cell). He used Kelvin–Helmholtz instability wavelength λ_{KH} , along with the interface between the idealized cylindrical vapor flow channel and liquid, and also introduced the Rayleigh–Taylor instability wavelength to evaluate the onset of hydrodynamic instability. The final relation is written in terms of the Rayleigh–Taylor wavelength as [11]

$$q_{CHF} = \Delta h_{lg} \left(\frac{2\pi^3 a^3 \sigma \rho_g}{9\lambda_{RT}} \right)^{1/2} \quad (4)$$

Zuber uses $\lambda_{KH} = 2\pi a\lambda_b = 9a\lambda_{RT}$, and chooses $a = 1/4$ for the plain surface.

Here we suggest the reason why the thin, uniform coating q_{CHF} is 1.8 times (here we approximate this to 2) as high as that of the plain surface. We postulate that either the Rayleigh–Taylor wavelength λ_{RT} decreases by 1/4 of the wavelength for plain surface given by Eq. (1), as shown in Fig. 6(a), or that a increases by $2^{2/3}$ of that for plain surface as shown in Fig. 6(b).

The thin, uniform particle coating provides sites for a stable vapor formation at the top of the coating. The vapor–liquid interface represents a collective (statistical) modulation characterized by the pore spacing and the vapor departure sites. Using the Zuber model, this apparent decrease in the critical wavelength can be attributed to the higher density of vapor columns leaving the interface. These vapor columns may also cover a larger fraction of the surface area.

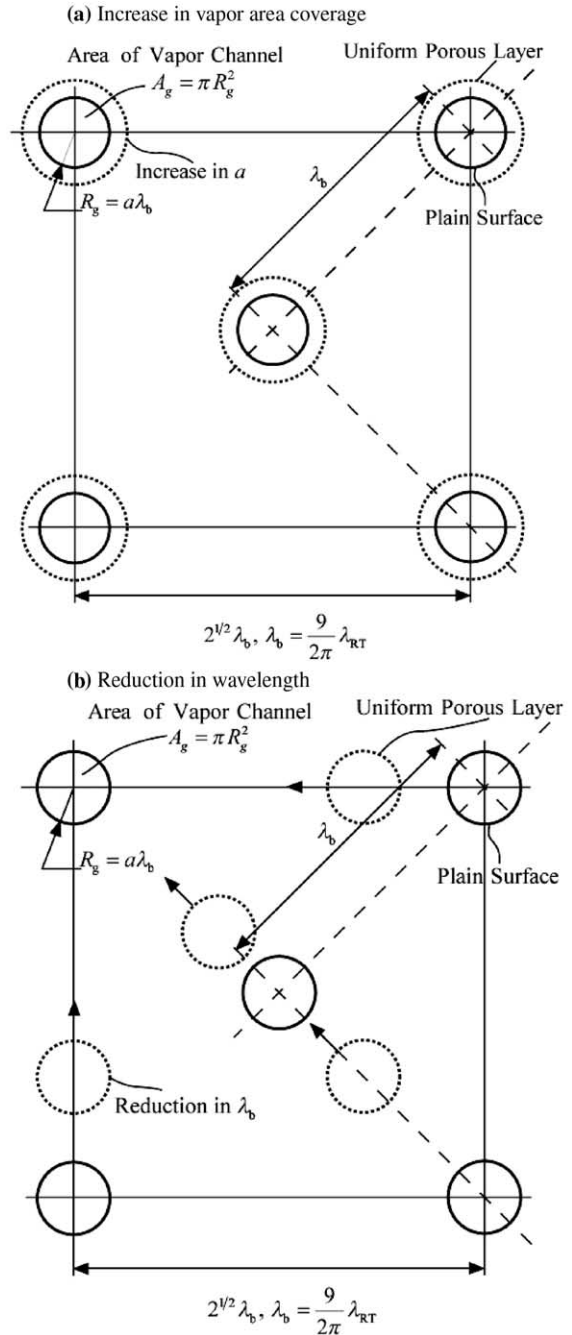


Fig. 6. The areas covered by liquid and vapor in the Zuber hydrodynamic stability model [11]. (a) The suggested increase in the fraction of area covered by vapor, (b) the suggested decrease in the wavelength.

Acknowledgements

Kent Pruss, University of Michigan, has provided excellent machining assistance. Pablo D. Quinones, University of Michigan, started this project and made improvements of the experimental apparatus. Scott G. LITER, GE Global Research Center, had built the experimental apparatus and has helped with the interpretation of the results. Special thanks to Olli Naukkarinen of Advanced Heat

Transfer, LLC, and Petri Rissanen of Outokumpu (Finland) for the brazed, uniform porous coatings.

References

- [1] A.E. Bergles, M.C. Chyu, Characteristics of nucleate pool boiling from porous metallic coatings, *ASME J. Heat Transfer* 104 (1982) 279–285.
- [2] J.R. Thome, *Enhanced Boiling Heat Transfer*, Hemisphere, New York, 1990.
- [3] J.Y. Chang, S.M. You, Enhanced boiling heat transfer from micro-porous surfaces: effects of a coating composition and method, *Int. J. Heat Mass Transfer* 40 (18) (1997) 4449–4460.
- [4] N.H. Afgan, L.A. Jovic, S.A. Kovalev, V.A. Lenykov, Boiling heat transfer from surfaces with porous layers, *Int. J. Heat Mass Transfer* 28 (2) (1985) 415–422.
- [5] K. Nishikawa, T. Ito, K. Tanaka, Augmented heat transfer by nucleate boiling at prepared surfaces, in: *Proceedings of the 1983 ASME–JSME Thermal Engineering Conference*, vol. 1, 1983, pp. 387–393.
- [6] R. Webb, *Principles of Enhanced Heat Transfer*, Wiley, New York, NY, 1993.
- [7] S.A. Kovalyo, S.L. Soloviyov, Heat transfer and critical heat fluxes in boiling on a porous surface, *Heat Transfer Sov. Res.* 22 (3) (1990) 364–375.
- [8] S.L. Soloviyov, Liquid evaporation heat transfer on a porous surface, *Heat Transfer Sov. Res.* 18 (3) (1986) 58–64.
- [9] S.M. Lu, R.H. Chang, Pool boiling from a surface with a porous layer, *AIChE J.* 33 (11) (1987) 1813–1828.
- [10] S.P. Malysenko, Features of heat transfer with boiling on surfaces with porous coatings, *Therm. Eng.* 38 (2) (1991) 81–88.
- [11] S.G. Liter, M. Kaviany, Pool-boiling CHF enhancement by modulated porous-layer coating: theory and experiment, *Int. J. Heat Mass Transfer* 44 (2001) 4287–4311.
- [12] N. Zuber, Hydrodynamic aspects of boiling heat transfer, AECU-4439, *Physics and Mathematics*, US Atomic Energy Commission, 1959.
- [13] R.L. Webb, Nucleate boiling on porous coated surfaces, *Heat Transfer Eng.* 4 (3–4) (1983) 71–82.
- [14] Y.V. Polezhaev, S.A. Kovalev, Modelling heat transfer with boiling on porous structures, *Therm. Eng.* 37 (12) (1990) 617–620.
- [15] M. Kaviany, *Principles of Heat Transfer in Porous Media*, second ed., Springer, New York, 1999.